

# FM-fMRI: Event Conditioned Flow Matching for Rest-to-Task fMRI Time-Series Synthesis

Peiyu Duan<sup>1</sup>, Jiyao Wang<sup>1</sup>, Nicha C. Dvornek<sup>1,2</sup>,  
Junlin Yang<sup>2</sup>, Ziqi Gao<sup>1</sup>, Lawrence H. Staib<sup>1,2</sup>, James S. Duncan<sup>1,2,3</sup>

<sup>1</sup> Department of Biomedical Engineering,

<sup>2</sup> Department of Radiology & Biomedical Imaging,

<sup>3</sup> Department of Electrical Engineering

Yale University, New Haven, CT, USA

camille.duan@yale.edu

**Abstract.** Task-based fMRI provides a direct readout of task-evoked neural dynamics, but it is expensive and difficult to acquire at scale, motivating rest-to-task synthesis from widely available resting-state fMRI (rsfMRI). We propose **FM-fMRI**, an **event-conditioned flow-matching** model that learns a continuous-time conditional vector field to generate task ROI time series from a subject’s rsfMRI and the task event information. The formulation enables fast ODE-based sampling and flexible conditioning over heterogeneous event schedules. Rather than optimizing for pointwise reconstruction, we evaluated generated signals using complementary criteria that probe temporal and spectral structure, subject and group-level connectome consistency, and distributional alignment. On the public Human Connectome Project and internal Biopoint autism cohort, FM-fMRI achieves the strongest spectral and connectivity agreement and improved distribution-level matching over conditional diffusion, generative adversarial networks (GANs), and variational autoencoders (VAEs) baselines. Furthermore, we augment the BioPoint cohort by synthesizing task-fMRI ROI time series with our method, improving downstream autism classification and demonstrating practical utility in data-limited clinical settings. The code will be available on GitHub.

**Keywords:** Functional MRI · Rest-to-Task Generation · Flow Matching · Event Conditioning · Functional Connectivity · Time-Series Synthesis

## 1 Introduction

Task-based functional Magnetic Resonance Imaging (tfMRI) is a primary tool for quantifying how the brain reconfigures under controlled cognitive and affective demands, which can expose disorder-related alterations and compensatory dynamics, supporting more sensitive disease identification than resting state fMRI (rsfMRI) [29][27]. However, it is expensive and operationally fragile due to its strict experimental control, longer scan sessions, and sustained subject engagement. These constraints make tfMRI difficult to collect at scale and particularly

challenging in pediatric, aging, and clinical cohorts. rsfMRI is comparatively easy to acquire and widely available, motivating rest-to-task generation that synthesizes task-evoked signals from rsfMRI to broaden access to task-like measurements and enable data augmentation when tfMRI is scarce.

Existing rest-to-task approaches often map resting connectivity to task activation or contrast maps, with recent graph neural networks, convolutional architectures, and transformers improving predictive performance [22, 18, 16, 17, 10]. However, these formulations target static summaries rather than ROI-resolved task time series, and their deterministic objectives tend to regress toward conditional means, under-representing distributional variability and task-evoked dynamics. Generic multivariate time-series generators based on GANs, VAEs, and diffusion models can produce stochastic samples [30, 31, 19, 14], and neuroimaging-specific variants have begun to add task-alignment objectives for clinical prediction [11]; yet they remain challenging to control with experimental schedules and are seldom constrained to preserve fMRI structure such as low-frequency spectra and functional connectivity. What is needed is a generative framework that natively supports structured conditioning, efficient sampling, and differentiable constraint enforcement. Flow matching and rectified flow address this by learning continuous-time vector fields for conditional generation, enabling stable training and ODE-based sampling with a direct handle for incorporating structured, differentiable constraints [12, 15, 13]. Despite these advantages, flow-based formulations have rarely been explored for rest-conditioned, timing-controlled tfMRI time-series synthesis with explicit spectral and connectomic constraints.

We propose **FM-fMRI**, an **event-conditioned flow-matching** framework that synthesizes task-evoked ROI time series from a subject’s rsfMRI and experimental schedule timing via a learned continuous-time conditional vector field. Our main contributions are threefold: (1) an event-conditioned flow-matching formulation for rest-to-task fMRI generation; (2) evaluation prioritizing neurobiological realism, such as spectral, connectomic, and distribution-level validity, including recovery of group-level connectivity structure, over pointwise reconstruction; (3) strong synthesis performance across multiple tfMRI tasks with synthesized task signals improving downstream learning in data-limited clinical settings.

## 2 Method

We model rest-to-task synthesis as the conditional generation of task-evoked ROI time series given resting-state dynamics and experimental timing (Fig. 1),  $x_{\text{task}} \sim p_{\theta}(x_{\text{task}} | x_{\text{rest}}, e)$  where  $x_{\text{task}} \in \mathbb{R}^{T \times V}$  denotes ROI time series with  $V$  regions and  $T$  time points,  $x_{\text{rest}}$  is resting-state input, and  $e$  encodes task event information.

**Resting-state encoder** Given resting-state input  $x_{\text{rest}} \in \mathbb{R}^{T_{\text{rest}} \times V}$ , we extract a subject-specific context embedding  $c = f_{\text{enc}}(x_{\text{rest}})$  using a patch-based

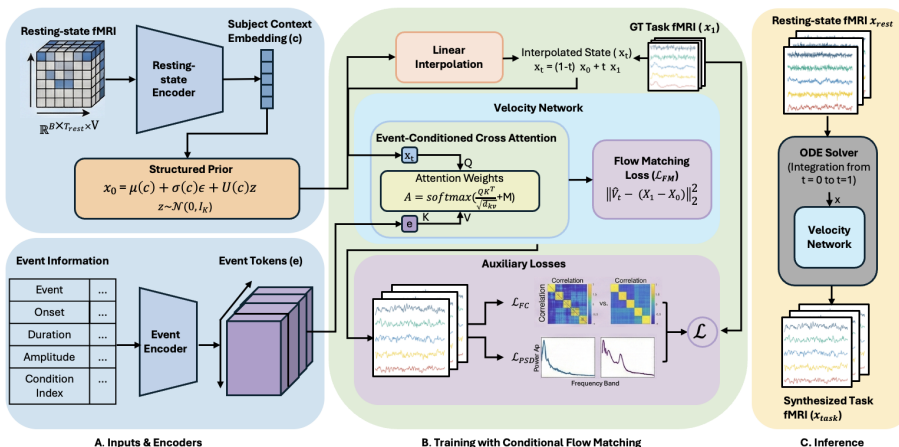


**Fig. 1. FM-fMRI overview.** (A) Inputs and encoders: resting-state ROI time series are encoded to parameterize a structured prior, while event information is encoded into event tokens; (B) Training: we learn an event-conditioned velocity field via cross-attention, optimized with flow-matching, connectivity and spectrum-aware objectives. (C) Inference: task time series trajectories are synthesized by integrating the learned ODE.

Transformer encoder. A prepended [CLS] token aggregates sequence information, and its final representation is used as the resting context.

**Structured prior** Rather than using a typical flow-matching setup initialized from isotropic Gaussian noise, we learn a subject context-dependent structured prior specific to the fMRI signal:

$$x_0 = \mu(c) + \sigma(c) \epsilon_{\text{colored}} + U(c)z \quad z \sim \mathcal{N}(0, I_K), \quad (1)$$

where  $\mu(c)$  and  $\sigma(c)$  are rest-conditioned per-ROI means and scale heads, and  $U(c) \in \mathbb{R}^{V \times K}$  is a rest-conditioned low-rank spatial factor with rank  $K = 8$  that captures structured cross-ROI covariance. The term  $\epsilon_{\text{colored}}$  is a temporal template with the power spectral density proportional to  $1/f$ , to better capture the elevated low-frequency power of fMRI signals [1], and stabilize training.

**Task fMRI Event token** Task event information is derived from FSL-style event timing files [5], which contain information regarding the types of tasks performed  $s$ , the time duration  $d$ , stimulus amplitude  $a$ , and task onset  $o$ . For the  $k$ -th event, we parse the information into tuples  $(o_k, d_k, a_k, s_k)$ . We convert  $o_k, d_k$  to TR units (divided by TR) and  $z$ -score  $a_k$ . The task event token ( $e$ ) in Fig.1 is embedded as

$$e_k = \phi_{\text{MLP}}([o_k, d_k, a_k]) + E_{\text{cond}}(s_k), \quad (2)$$

where  $\phi_{\text{MLP}}$  projects continuous timing features and  $E_{\text{cond}}$  is a learned embedding for the task event type.

**Event-conditioned cross-attention** To allow time-specific modulation by experimental structure, event tokens are incorporated through cross-attention within the velocity network [25]. Queries are computed from the linear projection of the current state,  $Q = W_q x_t$ , while keys and values are derived from event tokens  $K = W_k e$ ,  $V = W_v e$ . Attention weights are  $A = \text{softmax}\left(\frac{QK^\top}{\sqrt{d_{\text{ev}}}} + M\right)$ , where  $M$  masks padded events. The resulting event context  $e_{\text{ctx}} = AV$  is concatenated with  $x_t$ , the resting context  $c$ , and the time embedding before predicting the velocity. This enables each time point to attend selectively to relevant task events.

**Conditional flow matching** We train a conditional velocity field  $v_\theta(t, x_t, c, e)$  using flow matching. Given prior samples  $x_0$  and real task signals  $x_1$ , we construct linear interpolants  $x_t = (1-t)x_0 + tx_1$ ,  $t \sim \mathcal{U}(0, 1)$  with target velocity  $v^*(x_t, t) = x_1 - x_0$ . The flow-matching objective is

$$\mathcal{L}_{\text{FM}} = \mathbb{E}_{t, x_0} \left[ \|v_\theta(t, x_t, c, e) - (x_1 - x_0)\|_2^2 \right]. \quad (3)$$

In practice,  $v_\theta$  is parameterized by a lightweight MLP applied pointwise over time: we concatenate  $x_t$ , the resting context  $c$ , a learned time embedding  $\psi(t)$ , and an event-derived context vector.

**Connectivity and spectrum-aware objectives** We add auxiliary losses to preserve neurophysiological structure beyond pointwise fidelity. For functional connectivity (FC), let  $R_{ij}(x)$  denote the Pearson correlation between ROI  $i$  and  $j$ ; we define a weighted FC loss which emphasizes preservation of strong task-relevant connections.

$$\mathcal{L}_{\text{FC}} = \sum_{i < j} w_{ij} (R_{ij}(\hat{x}_1) - R_{ij}(x_1))^2, \quad w_{ij} = |R_{ij}(x_1)|^2, \quad (4)$$

For spectral fidelity, let  $P_i(f) = |\mathcal{F}(x_i)(f)|^2$  denote the power spectrum of ROI  $i$ ; over a physiologically relevant band  $\mathcal{B}$  (0.01–0.05 Hz) [33], we use

$$\mathcal{L}_{\text{PSD}} = \sum_i \sum_{f \in \mathcal{B}} \left( \log P_i^{\hat{x}_1}(f) - \log P_i^{x_1}(f) \right)^2. \quad (5)$$

The overall training objective is  $\mathcal{L} = \mathcal{L}_{\text{FM}} + \lambda_{\text{FC}} \mathcal{L}_{\text{FC}} + \lambda_{\text{PSD}} \mathcal{L}_{\text{PSD}}$ .

We optimize all models with Adam (learning rate  $1 \times 10^{-3}$ ; weight decay  $1 \times 10^{-5}$ ) for 50 epochs and a batch size of 16. At test time, task trajectories are generated by integrating the learned ODE

$$\frac{dx}{dt} = v_\theta(t, x, c, e) \quad (6)$$

from  $t = 0$  to 1 using an explicit Euler fixed-step solver starting from the learned structured prior  $x_0$ , yielding  $x(1)$  as the synthesized task fMRI signal [2].

**Table 1.** Subject-level generation performance grouped by metric. Best values are bolded.

Metric	Model	Emotion	Gambling	Language	Motor	Relational	Social	WM
PSD ↓	TimeGAN[30]	2.0546	1.9923	1.9109	1.9390	1.9305	1.9179	1.9371
	TimeVAE[21]	2.0517	1.9721	1.8791	1.8829	1.8805	1.8560	1.9093
	Diffusion-TS[31]	4.0047	4.0942	3.9848	4.0620	3.9983	4.1018	3.9994
	DDPM[4]	1.7793	1.6921	1.5944	1.6350	1.6719	1.7894	1.4799
	LSTM-GAN[32]	2.1006	2.0959	1.9916	1.9727	2.0687	2.1236	1.8706
	<b>FM-fMRI</b>	<b>1.6001</b>	<b>1.5399</b>	<b>1.4222</b>	<b>1.3634</b>	<b>1.4305</b>	<b>1.5601</b>	<b>1.3189</b>
FC sim. ↑	TimeGAN[30]	0.2546	0.2229	0.2307	0.1723	0.2473	0.2630	0.2296
	TimeVAE[21]	0.2795	0.2653	0.2640	0.2433	0.2942	0.3078	0.2580
	Diffusion-TS[31]	0.0442	0.0168	0.0109	0.0026	0.0123	0.0078	0.0073
	DDPM[4]	0.2677	0.2618	0.2454	0.2429	0.2056	0.2087	0.2274
	LSTM-GAN[32]	0.2935	0.1432	0.2305	0.2439	0.2593	0.3399	0.1968
	<b>FM-fMRI</b>	<b>0.5684</b>	<b>0.5455</b>	<b>0.5272</b>	<b>0.5302</b>	<b>0.5606</b>	<b>0.6046</b>	<b>0.5366</b>
cFID ↓	TimeGAN[30]	98.06	114.91	127.31	151.15	121.47	120.66	116.97
	TimeVAE[21]	105.62	116.22	129.48	154.58	127.17	123.59	118.43
	Diffusion-TS[31]	177.12	188.78	194.03	220.74	194.29	202.80	189.29
	DDPM[4]	35.69	41.16	39.59	44.66	40.43	46.80	48.78
	LSTM-GAN[32]	113.76	257.37	128.54	142.30	159.14	102.28	184.56
	<b>FM-fMRI</b>	<b>24.1311</b>	<b>30.6712</b>	<b>37.5067</b>	<b>35.5717</b>	<b>29.8250</b>	<b>30.7688</b>	<b>39.9683</b>
MAE ↓	TimeGAN[30]	0.7676	0.7658	0.7662	0.7702	0.7551	0.7527	0.7670
	TimeVAE[21]	<b>0.7661</b>	<b>0.7620</b>	<b>0.7562</b>	<b>0.7532</b>	<b>0.7471</b>	<b>0.7431</b>	<b>0.7529</b>
	Diffusion-TS[31]	0.9393	0.9382	0.9315	0.9445	0.9351	0.9392	0.9174
	DDPM[4]	0.8016	0.8005	0.8040	0.8019	0.8002	0.8029	0.8025
	LSTM-GAN[32]	0.7797	0.7904	0.7877	0.7785	0.7888	0.7785	0.7913
	<b>FM-fMRI</b>	0.9342	0.9413	0.9508	0.9599	0.9588	0.9569	0.9437
P@5% ↑	TimeGAN[30]	0.2173	0.2186	0.2289	0.1775	0.2986	0.1731	0.1809
	TimeVAE[21]	0.2215	0.2130	0.2329	0.2157	0.3010	0.2046	0.1904
	Diffusion-TS[31]	0.1599	0.2426	0.2318	0.2361	0.2175	0.1748	0.3084
	DDPM[4]	0.2641	0.2506	0.2137	0.2210	0.2181	0.2208	0.2635
	LSTM-GAN[32]	0.2394	0.1231	0.1240	0.1836	0.1485	0.2342	0.1082
	<b>FM-fMRI</b>	<b>0.4617</b>	<b>0.4329</b>	<b>0.4352</b>	<b>0.4404</b>	<b>0.5000</b>	<b>0.4825</b>	<b>0.4535</b>

### 3 Experiments and Results

**Datasets and Data Preprocessing** We evaluate rest-to-task synthesis with two cohorts that span large-scale normative fMRI and a clinical task-fMRI setting. For the Human Connectome Project (HCP) [24], we use 1,025 subjects with paired rsfMRI and tfMRI across seven paradigms. For each run, we extract regional mean BOLD time series using the AAL atlas [23], yielding paired resting inputs and task targets. For FM-fMRI, we additionally leverage the task timing files, which contain stimulus onsets, duration, and conditioning information. To assess generalization beyond HCP, we also evaluate on the Biopoint cohort [6] (118 participants; 75 with autism and 43 controls), extracting ROI time series with the Shen268 atlas [20]. For both datasets, we use subject-disjoint splits of 70% for training, 15% for validation, 15% for test to prevent data leakage.

#### 3.1 Baseline and Metrics

We benchmark FM-fMRI against conditional DDPM [4], Diffusion-TS [31], TimeVAE [8, 21], TimeGAN [30], and LSTM-GAN [32], all conditioned on a resting-state context embedding. We use tfMRI-aligned metrics: PSD [28] discrepancy to assess preservation of the spectrum, FC similarity calculated by the

**Table 2.** Biopoint subject-level generation performance. Best values are bolded.

Model	MAE ↓	PSD ↓	FC sim. ↑	FC P@5% ↑	cFID ↓
TimeGAN[30]	0.7667	2.5819	0.1672	0.0977	168.76
TimeVAE[21]	<b>0.7659</b>	2.5791	0.2679	0.1688	118.60
Diffusion-TS[31]	1.0650	2.6324	0.0940	0.0855	116.99
DDPM[4]	0.8218	2.3643	0.1402	0.1344	104.53
LSTM-GAN[32]	0.7672	2.5852	0.0012	0.0532	455.66
<b>FM-fMRI</b>	0.7923	<b>2.3445</b>	<b>0.3508</b>	<b>0.2436</b>	<b>43.32</b>

Pearson correlation of the FC map, top-5% edge recovery (P@5%) to evaluate connectome structure, and cFID [3] to quantify conditional distributional alignment in FC space. Since rest-to-task synthesis is many-to-many, we prioritize second-order structure and report MAE only as an amplitude sanity check.

**Task fMRI Synthesis on HCP and Biopoint** HCP results in Table 1 highlight the distinction between pointwise reconstruction fidelity and neurophysiological realism in rest-to-task synthesis. Methods such as TimeVAE achieve the lowest MAE, consistent with variance-shrinking conditional-mean predictions that match average trajectories yet over-smooth task-evoked variability and distort spectral or connectomic structure shown in Fig. 2. FM-fMRI exhibits higher MAE than reconstruction-focused baselines, which is expected given that it is not optimized for strict pointwise waveform matching. Instead, FM-fMRI preserves realistic low-frequency power and cross-ROI covariance geometry, leading to improved PSD and FC realism and stronger conditional population alignment, which better reflects downstream connectivity and group-level analyses.

On Biopoint (Table 2), despite cohort and atlas differences, the same pattern holds: baseline rankings vary across MAE and PSD, whereas FM-fMRI consistently yields the strongest connectivity realism and distributional matching, supporting robustness under dataset and atlas shifts.

### 3.2 Ablation: Event Conditioning and Auxiliary Objectives

Table 3 ablates event token and auxiliary connectivity (Aux) losses on HCP. The full model with event information input and connectivity objective is the most reliable configuration, achieving the best or near-best performance across tasks on structure-aware metrics, indicating that task-timing cues and explicit neurophysiological regularization are jointly necessary for realistic synthesis. The ablation also highlights complementary effects: Aux alone drives substantial gains in spectral and connectivity fidelity relative to the baseline, whereas event information alone often improves pointwise alignment but does not consistently enhance FC-space distributional matching. Together, these results reinforce that MAE is insufficient to characterize rest-to-task realism and that combining event token conditioning with spectrum/FC-aware objectives yields the most consistent improvements on metrics aligned with downstream neuroimaging analyses.

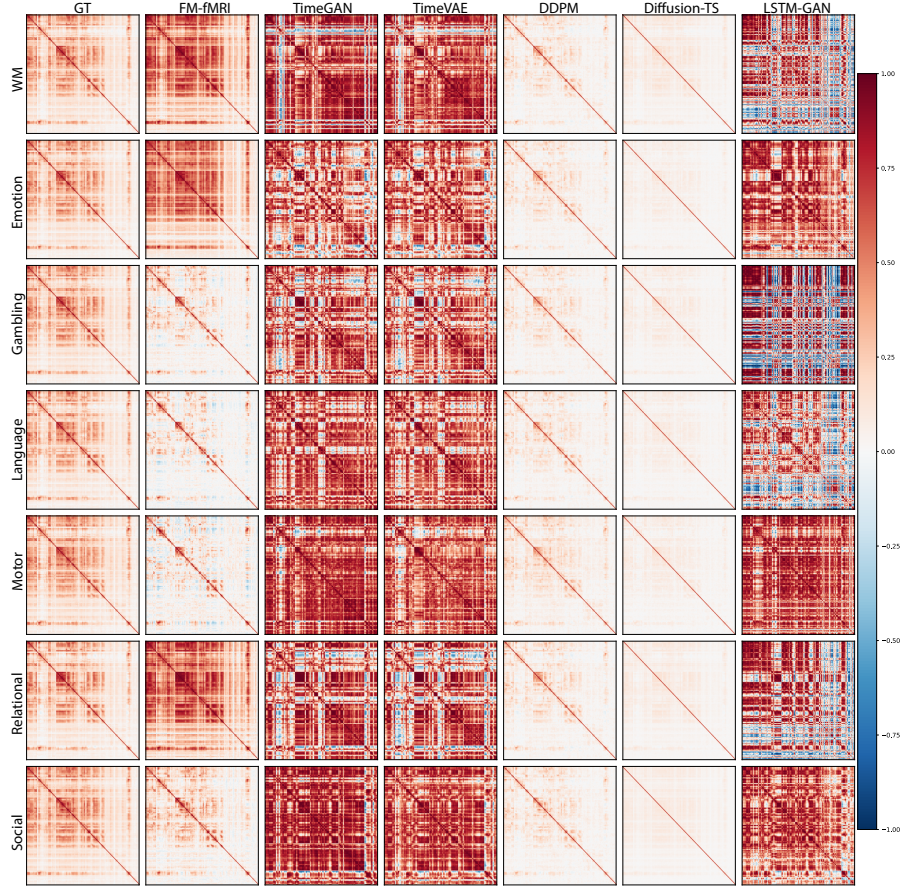


**Fig. 2.** Group-level FC comparison on all HCP tasks.

### 3.3 Downstream Classification Augmentation on Biopoint

We assess downstream utility on Biopoint autism classification with three graph-based models under three training regimes: rsfMRI-only, tfMRI-only without augmentation, and tfMRI augmented with our proposed model. Synthetic tfMRI is generated for all biopoint cohort in the training split using its rsfMRI without access to validation/test subjects. The final performance is reported on a held-out test set (Table 4). tfMRI-only generally surpasses rsfMRI-only performance, implying added discriminative information in task-evoked signals, except for the lowest-capacity classifier. Across all classifiers and metrics, augmentation with our synthesized signals yields consistent performance gains, with the largest improvements for the most state-of-the-art model (STAGIN) [7]. These results

**Table 3.** Ablation results on Event information and Aux losses. Best values are bolded.

Task	Event	Aux	MAE ↓	PSD ↓	FC Sim ↑	P@5 ↑	cFID ↓
WM	–	–	0.8625	2.0286	0.2665	0.2528	44.1144
	–	✓	0.9425	1.3688	0.5025	0.4111	41.8149
	✓	–	<b>0.8549</b>	2.0158	0.3183	0.2682	64.9692
	✓	✓	0.9437	<b>1.3189</b>	<b>0.5366</b>	<b>0.4535</b>	<b>39.9683</b>
Emotion	–	–	<b>0.8184</b>	2.0238	0.3391	0.2879	33.0135
	–	✓	0.9436	1.6475	0.5095	0.4077	44.4805
	✓	–	0.8448	1.9540	0.4219	0.2977	65.4704
	✓	✓	0.9342	<b>1.6001</b>	<b>0.5684</b>	<b>0.4617</b>	<b>24.1311</b>
Gambling	–	–	0.8297	1.9546	0.2472	0.2391	47.6530
	–	✓	0.9382	1.6074	0.5039	0.3949	46.1616
	✓	–	<b>0.8262</b>	1.9416	0.4720	0.3613	37.1983
	✓	✓	0.9413	<b>1.5399</b>	<b>0.5455</b>	<b>0.4329</b>	<b>30.6712</b>
Language	–	–	0.8535	1.9730	0.2875	0.2669	38.2063
	–	✓	0.9602	1.4749	0.5007	0.3944	60.30
	✓	–	<b>0.8505</b>	1.9669	0.3543	0.2867	59.6663
	✓	✓	0.9508	<b>1.4222</b>	<b>0.5272</b>	<b>0.4352</b>	<b>37.5067</b>
Motor	–	–	0.8805	2.1643	0.2380	0.2408	50.4327
	–	✓	0.9604	1.7153	0.4886	0.4124	39.5460
	✓	–	<b>0.8748</b>	2.1286	0.2966	0.2576	67.4445
	✓	✓	0.9599	<b>1.3634</b>	<b>0.5302</b>	<b>0.4404</b>	<b>35.5717</b>
Relational	–	–	0.8544	1.9700	0.2986	0.2733	40.0110
	–	✓	0.9539	1.4997	0.5064	0.4559	45.1027
	✓	–	<b>0.8516</b>	1.9615	0.3614	0.2894	61.1435
	✓	✓	0.9588	<b>1.4305</b>	<b>0.5606</b>	<b>0.5000</b>	<b>29.8250</b>
Social	–	–	<b>0.8588</b>	2.0207	0.3265	0.2718	64.3218
	–	✓	0.9763	1.6057	0.5568	0.4313	47.2015
	✓	–	0.8639	2.0199	0.2685	0.2539	43.3593
	✓	✓	0.9569	<b>1.5601</b>	<b>0.6046</b>	<b>0.4825</b>	<b>30.7688</b>

demonstrate that generative rest-to-task modeling provides a practical and reliable augmentation strategy for data-scarce clinical cohorts.

**Table 4.** Biopoint ASD classification performance under three settings: rest-only, task-based with and w/o augmentation. Best performance is bolded.

Model	Rest-only				Task w/o Augmentation				Task with Augmentation			
	Acc. ↑	F1 ↑	AUC ↑	Sens. ↑	Acc. ↑	F1 ↑	AUC ↑	Sens. ↑	Acc. ↑	F1 ↑	AUC ↑	Sens. ↑
GCN[9]	0.4583	0.5185	0.5333	0.4667	0.4583	0.5517	0.4963	0.5333	<b>0.6250</b>	<b>0.6897</b>	<b>0.6741</b>	<b>0.6667</b>
GAT[26]	0.5417	0.5926	0.6074	0.5333	0.5833	0.6154	0.6074	0.5333	<b>0.6250</b>	<b>0.6400</b>	<b>0.7259</b>	<b>0.5333</b>
STAGIN[7]	0.5833	0.6875	0.5037	0.7333	0.6667	0.7333	0.6741	0.7333	<b>0.7500</b>	<b>0.7609</b>	<b>0.7481</b>	<b>0.8667</b>

## 4 Conclusion and Discussion

We presented **FM-fMRI**, an event-conditioned flow-matching model for rest-to-task fMRI time-series synthesis. Across seven HCP tasks, FM-fMRI delivers the best spectral fidelity, functional-connectivity recovery, and FC-based distributional alignment, underscoring the importance of structure-aware evaluation

beyond pointwise reconstruction. Ablations confirm that event conditioning and connectivity regularization are both necessary for distribution-level performance. On the data-limited Biopoint autism cohort, synthesized task-like signals consistently improve downstream autism classification, with the largest gains for STAGIN. FM-fMRI remains effective across cohorts and atlas choices. Future work will extend conditioning and test cross-site robustness and calibration.

## References

1. Biswal, B., Yetkin, F.Z., Haughton, V.M., Hyde, J.S.: Functional connectivity in the motor cortex of resting human brain using echo-planar MRI. *Magnetic Resonance in Medicine* **34**(4), 537–541 (1995). <https://doi.org/10.1002/mrm.1910340409>
2. Chen, R.T.Q., Rubanova, Y., Bettencourt, J., Duvenaud, D.K.: Neural ordinary differential equations. In: *Advances in Neural Information Processing Systems*. vol. 31 (2018)
3. Heusel, M., Ramsauer, H., Unterthiner, T., Nessler, B., Hochreiter, S.: Gans trained by a two time-scale update rule converge to a local nash equilibrium. In: *Advances in Neural Information Processing Systems*. vol. 30 (2017)
4. Ho, J., Jain, A., Abbeel, P.: Denoising diffusion probabilistic models. In: *Advances in Neural Information Processing Systems* (2020)
5. Jenkinson, M., Beckmann, C.F., Behrens, T.E.J., Woolrich, M.W., Smith, S.M.: FSL. *NeuroImage* **62**(2), 782–790 (2012). <https://doi.org/10.1016/j.neuroimage.2011.09.015>
6. Kaiser, M.D., Hudac, C.M., Shultz, S., Lee, S.M., Cheung, C., Berken, A.M., Deen, B., Pitskel, N.B., Sugrue, D.R., Voos, A.C., Saulnier, C.A., Ventola, P., Wolf, J.M., Klin, A., Vander Wyk, B.C., Pelphrey, K.A.: Neural signatures of autism. *Proceedings of the National Academy of Sciences* **107**(49), 21223–21228 (2010). <https://doi.org/10.1073/pnas.1010412107>
7. Kim, B.H., Ye, J.C., Kim, J.J.: Learning dynamic graph representation of brain connectome with spatio-temporal attention. In: *Advances in Neural Information Processing Systems*. vol. 34, pp. 4314–4327 (2021)
8. Kingma, D.P., Welling, M.: Auto-encoding variational bayes. In: *International Conference on Learning Representations* (2014)
9. Kipf, T.N., Welling, M.: Semi-supervised classification with graph convolutional networks. In: *5th International Conference on Learning Representations (ICLR) 2017, Conference Track Proceedings* (2017)
10. Kwon, J., Seo, J., Wang, H., Moon, T., Yoo, S., Cha, J.: Predicting task-related brain activity from resting-state brain dynamics with fMRI transformer. *Imaging Neuroscience* (2025). [https://doi.org/10.1162/imag\\_a\\_00440](https://doi.org/10.1162/imag_a_00440)
11. Li, Y., Wu, X., Zhang, X., Jiang, H., Wu, W., Shen, D., Zhang, J.: Task-aligned fMRI generation model for brain disorder diagnosis. In: *Medical Image Computing and Computer Assisted Intervention – MICCAI 2025. Lecture Notes in Computer Science*, vol. 15971, pp. 638–648. Springer (2025). [https://doi.org/10.1007/978-3-032-05162-2\\_61](https://doi.org/10.1007/978-3-032-05162-2_61)
12. Lipman, Y., Chen, R.T.Q., Ben-Hamu, H., Nickel, M., Le, M.: Flow matching for generative modeling. *arXiv* (2022)
13. Lipman, Y., et al.: A guide to flow matching and its extensions. *arXiv* (2024)

14. Liu, X., et al.: Retrieval-augmented diffusion models for time series generation. In: *Advances in Neural Information Processing Systems* (2024)
15. Liu, X., Gong, C., Liu, Q.: Rectified flow: A marginal preserving approach to optimal transport. *arXiv* (2022)
16. Ngo, G., Huang, Y., Zhang, Y., Raj, A.: Connectomic deep learning for predicting functional activation from resting-state fMRI. *arXiv* (2020)
17. Ngo, G., Seeley, W.W., Raj, A.: Predicting task activation from resting-state functional connectivity using deep learning. *NeuroImage* **246**, 118703 (2022)
18. Parker Jones, O., Voets, N.L., Adcock, J.E., Stacey, R., Jbabdi, S.: Resting connectivity predicts task activation in pre-surgical populations. *NeuroImage: Clinical* **13**, 378–385 (2017). <https://doi.org/10.1016/j.nicl.2016.12.028>
19. Shen, L., Chen, W., Kwok, J.T.: Multi-resolution diffusion models for time series forecasting. In: *International Conference on Learning Representations* (2024)
20. Shen, X., Tokoglu, F., Papademetris, X., Constable, R.T.: Groupwise whole-brain parcellation from resting-state fMRI data for network node identification. *NeuroImage* **82**, 403–415 (2013)
21. Sohn, K., Lee, H., Yan, X.: Learning structured output representation using deep conditional generative models. In: *Advances in Neural Information Processing Systems* (2015)
22. Tavor, I., Jones, O.P., Mars, R.B., Smith, S.M., Behrens, T.E., Jbabdi, S.: Task-free MRI predicts individual differences in brain activity during task performance. *Science* **352**(6282), 216–220 (2016)
23. Tzourio-Mazoyer, N., Landeau, B., Papathanassiou, D., Crivello, F., Etard, O., Delcroix, N., Mazoyer, B., Joliot, M.: Automated anatomical labeling of activations in SPM using a macroscopic anatomical parcellation of the MNI MRI single-subject brain. *NeuroImage* **15**(1), 273–289 (2002)
24. Van Essen, D.C., Ugurbil, K., Auerbach, E., Barch, D., Behrens, T.E.J., Bucholz, R., Chang, A., Chen, L., Corbetta, M., Curtiss, S.W., Della Penna, S., Feinberg, D., Glasser, M.F., Harel, N., Heath, A.C., Larson-Prior, L., Marcus, D., Michalareas, G., Moeller, S., Oostenveld, R., Petersen, S.E., Prior, F., Schlaggar, B.L., Smith, S.M., Snyder, A.Z., Xu, J., Yacoub, E.: The human connectome project: A data acquisition perspective. *NeuroImage* **62**(4), 2222–2231 (2012). <https://doi.org/10.1016/j.neuroimage.2012.02.018>
25. Vaswani, A., Shazeer, N., Parmar, N., Uszkoreit, J., Jones, L., Gomez, A.N., Kaiser, L., Polosukhin, I.: Attention is all you need. In: *Advances in Neural Information Processing Systems*. vol. 30 (2017)
26. Velickovic, P., Cucurull, G., Casanova, A., Romero, A., Liò, P., Bengio, Y.: Graph attention networks. In: *6th International Conference on Learning Representations (ICLR) 2018, Conference Track Proceedings* (2018)
27. Wang, J., Dvornek, N.C., Duan, P., Staib, L.H., Ventola, P., Duncan, J.S.: STNAGNN: Spatiotemporal node attention graph neural network for task-based fMRI analysis. *arXiv* (2024)
28. Welch, P.D.: The use of fast fourier transform for the estimation of power spectra: A method based on time averaging over short, modified periodograms. *IEEE Transactions on Audio and Electroacoustics* **15**(2), 70–73 (1967)
29. Woo, C.W., Chang, L.J., Lindquist, M.A., Wager, T.D.: Building better biomarkers: brain models in translational neuroimaging. *Nature Neuroscience* **20**(3), 365–377 (Mar 2017). <https://doi.org/10.1038/nn.4478>, epub 2017-02-23
30. Yoon, J., Jarrett, D., van der Schaar, M.: Time-series generative adversarial networks. In: *Advances in Neural Information Processing Systems* (2019)

31. Yuan, Y., et al.: Diffusion models for time series generation. In: International Conference on Learning Representations (2024)
32. Zhu, G., Zhao, H., Liu, H., Sun, H.: A novel LSTM-GAN algorithm for time series anomaly detection. In: 2019 Prognostics and System Health Management Conference. pp. 1–6. IEEE (2019)
33. Zuo, X.N., et al.: The oscillating brain: Complex and reliable. *NeuroImage* **49**(2), 1432–1445 (2010). <https://doi.org/10.1016/j.neuroimage.2009.09.037>